THE JOURNAL OF BIOLOGICAL CHEMISTRY VOL. 283, NO. 7, pp. 4295–4303, February 15, 2008

GDP-4-Keto-6-deoxy-D-mannose 3-Dehydratase, Accommodating a Sugar Substrate in the Active Site*

Received for publication, October 29, 2007, and in revised form, November 21, 2007 Published, JBC Papers in Press, November 28, 2007, DOI 10.1074/jbc.M708893200

Paul D. Cook and Hazel M. Holden[1]

From the Department of Biochemistry, University of Wisconsin, Madison, Wisconsin 53706-1544

Colitose is a dideoxysugar found in the O-antigen of the lipopolysaccharide that coats the outer membrane of some Gram-negative bacteria. Four enzymes are required for its production starting from D-mannose-1-phosphate and GTP. The focus of this investigation is GDP-4-keto-6-deoxy-D-mannose 3-dehydratase or ColD, which catalyzes the removal of the C3′-hydroxyl group from GDP-4-keto-6-deoxymannose. The enzyme is pyridoxal 5′-phosphate-dependent, but unlike most of these proteins, the conserved lysine residue that covalently holds the cofactor in the active site is replaced with a histidine residue. Here we describe the three-dimensional structure of ColD, determined to 1.7 Å resolution, whereby the active site histidine has been replaced with an asparagine residue. For this investigation, crystals of the site-directed mutant protein were grown in the presence of GDP-4-amino-4,6-dideoxy-D-mannose (GDP-perosamine). The electron density map clearly reveals the presence of the sugar analog trapped in the active site as an external aldimine. The active site is positioned between the two subunits of the dimer. Whereas the pyrophosphoryl groups of the ligand are anchored to the protein via Arg-219 and Arg-331, the hydroxyl groups of the hexose only lie within hydrogen bonding distance to ordered water molecules. Interestingly, the hexose moiety of the ligand adopts a boat rather than the typically observed chair conformation. Activity assays demonstrate that this mutant protein cannot catalyze the dehydration step. Additionally, we report data revealing that wild-type ColD is able to catalyze the production of GDP-4-keto-3,6-dideoxymannose using GDP-perosamine instead of GDP-4-keto-6-deoxymannose as a substrate.

The lipopolysaccharide (LPS)[2] of Gram-negative bacteria is the major structural component of the outer membrane, where it has been estimated to occupy ~75% of the total bacterial surface area (1). As the name implies, the LPS is a complex glycoconjugate that varies from species to species in specific content, but in all cases it is thought to provide a permeability barrier to hydrophobic or negatively charged molecules. Conceptually, the LPS can be thought of in terms of three regions: lipid A, the core oligosaccharide, and the *O*-specific polysaccharide (2). Lipid A, which anchors the sugar components of the LPS to the bacterial cell outer membrane, has been implicated in the toxicity associated with Gram-negative infections. Unlike the typical lipids attached to glycerol, however, lipid A is a glucosamine-based phospholipid (2) and is connected to the core polysaccharide of the LPS via 3-deoxy-D-*manno*-octulosonic acid. Besides 3-deoxy-D-*manno*-octulosonic acid, the core polysaccharide usually contains heptose (typically L-*glycero*-D-*manno*-heptose), galactose, glucose, and *N*-acetylglucosamine. The *O*-specific polysaccharide region, which extends farthest away from the bacterium, displays the most variation from species to species. This region, also referred to as the O-antigen, consists of repeating units, which typically contain 3–5 sugars. Indeed, the carbohydrate differences within the O-antigens contribute to the wide varieties of bacterial strains observed in nature. The O-antigens often contain some quite remarkable and unusual dideoxysugars, including tyvelose, paratose, abequose, perosamine, and colitose. These sugars are added to the LPS via the action of glycosyltransferases, which employ nucleotide-linked derivatives, such as CDP-tyvelose or GDP-colitose, as substrates.

The research described here focuses on one of the enzymes involved in the production of GDP-colitose, namely GDP-4-keto-6-deoxy-D-mannose-3-dehydratase, hereafter referred to as ColD. As shown in Scheme 1, the biosynthetic pathway leading to the formation of GDP-colitose requires four different enzymes. ColD catalyzes the third step, which is the removal of the C3′-hydroxyl group from GDP-4-keto-6-deoxymannose. It requires pyridoxal 5′-phosphate (PLP) for activity, but unlike most PLP-dependent enzymes, the cofactor is not covalently attached to the protein via a lysine residue. In place of the lysine is His-188, and the functional form of the cofactor in ColD is PMP, which is derived from the reaction of PLP with L-glutamate.

Recently, a three-dimensional structural analysis of ColD was reported from this laboratory (3). This study revealed that ColD belongs to the well characterized aspartate aminotransferase superfamily. As shown in Fig. 1, each subunit of the dimeric enzyme is dominated by a mixed eight-stranded β-sheet flanked by eight α-helices. Additional β-strands and α-helices complete the overall tertiary structure of ColD. Amino acid residues from both subunits contribute to the active site regions of the dimer.

* This research was supported by National Institutes of Health Grant DK47814 (to H. M. H.). The costs of publication of this article were defrayed in part by the payment of page charges. This article must therefore be hereby marked "*advertisement*" in accordance with 18 U.S.C. Section 1734 solely to indicate this fact.

The atomic coordinates and structure factors (code 3B8X) have been deposited in the Protein Data Bank, Research Collaboratory for Structural Bioinformatics, Rutgers University, New Brunswick, NJ (http://www.rcsb.org/).

[1] To whom correspondence should be addressed. E-mail: Hazel_Holden@biochem.wisc.edu.

[2] The abbreviations used are: LPS, lipopolysaccharide; PLP, pyridoxal 5′-phosphate; ESI, electrospray ionization; MES, 4-morpholineethanesulfonic acid; PMP, pyridoxamine-5′-phosphate.

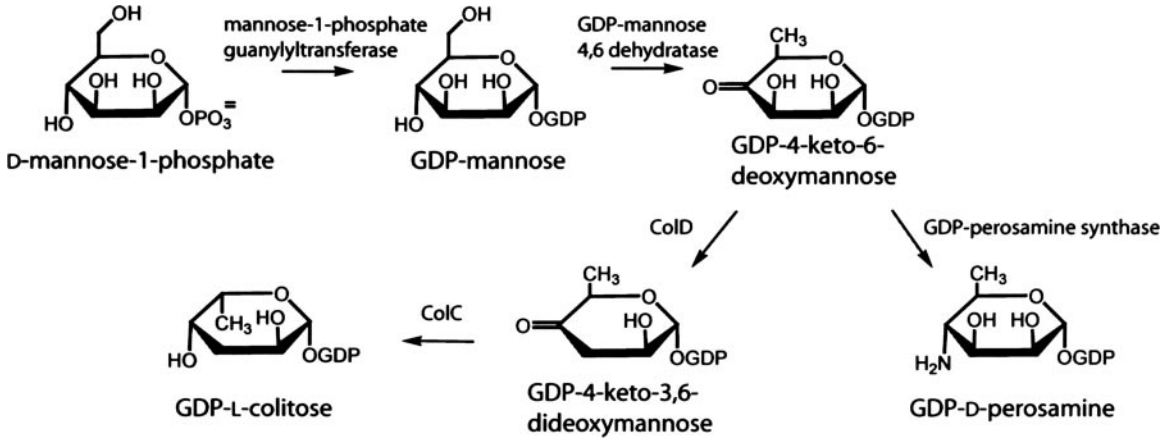

SCHEME 1. **Biosynthetic pathway leading to the formation of GDP-colitose and GDP-perosamine.**

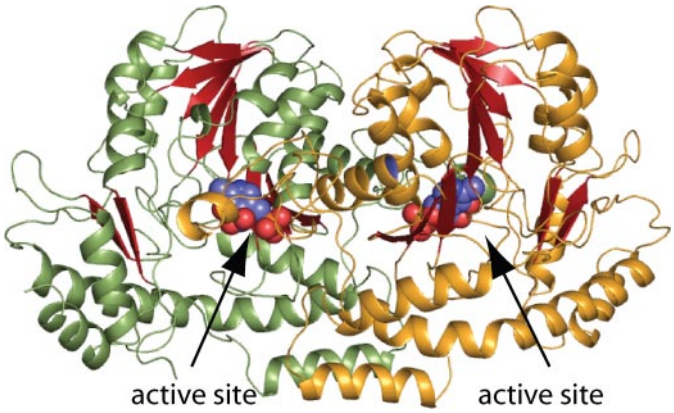

FIGURE 1. **Three-dimensional structure of the wild-type ColD dimer.** Subunits 1 and 2 are depicted in *green* and *yellow*, respectively. The β-strands in each subunit are highlighted in *red*. Each subunit contains a bound PLP cofactor, as indicated by the *space-filling representations*.

A possible catalytic mechanism for ColD, based on all presently available biochemical and structural data, is presented in Scheme 2 (3, 4). In the first step, a Schiff base is formed between the sugar C4′ and the PMP cofactor with the concomitant loss of a water molecule. This is referred to as the external aldimine. In the next step, the side chain of His-188 abstracts the *pro*R proton from the cofactor C4′ and delivers it to the sugar C3′-hydroxyl group, thereby facilitating its departure and the subsequent generation of a $\Delta^{3,4}$-aminomannoseen intermediate. This intermediate is hydrolyzed by a water molecule to yield free PLP and an aminated sugar moiety. It is thought that the hydrogen incorporated at the sugar C3′ in the next step of the mechanism is derived from the protonated form of His 188. Presently, it is not known whether the final expulsion of ammonia occurs on the enzyme or in solution.

Although the original structures of ColD defined the manner in which both the hydrated form of PLP and a glutamate-ketimine intermediate were accommodated within the active site pocket, crystallization experiments of ColD in the presence of its sugar substrate never led to clearly interpretable electron density for the ligand. Most likely, either the enzyme was active in the crystalline lattice and the product was being released, or the substrate, GDP-4-keto-6-deoxymannose, was unstable in the crystallization solutions.

In an effort to address the issue of substrate binding to ColD, we initiated a two-pronged approach. The first step was to prepare a site-directed mutant protein of ColD in which the active site base, His-188, was changed to an asparagine residue. The second step was to clone, overexpress, and purify GDP-perosamine synthase, which catalyzes the production of GDP-perosamine from GDP-4-keto-6-deoxymannose, the same substrate used by ColD (Scheme 1). Note that the difference between GDP-perosamine and the natural ColD substrate is the replacement of the keto group at C4′ with an amino functionality. The reasoning behind this was that GDP-perosamine might be more stable in the ColD crystallization conditions. In addition, if the proposed catalytic mechanism is correct as outlined in Scheme 2, then GDP-perosamine might react with PLP in the ColD active site to form a covalent intermediate.

By using this combined approach, we were able to trap a nucleotide-linked sugar in the active site of ColD. Here we describe the high resolution structural analysis of this ColD H188N-nucleotide-linked sugar complex. We also present activity assays demonstrating that this mutant form of the protein cannot function as a dehydratase. Finally, we demonstrate that the wild-type form of ColD can, in fact, catalyze the formation of GDP-4-keto-3,6-dideoxymannose using GDP-perosamine rather than GDP-4-keto-6-deoxymannose as a substrate, which further supports the proposed mechanism outlined in Scheme 2.

EXPERIMENTAL PROCEDURES

Cloning, Site-directed Mutagenesis, Protein Expression, and Purification of ColD H188N—The gene encoding ColD was isolated as previously described (3) and used to produce the ColD-pET28JT plasmid. His-188 was changed to an asparagine through site-directed mutagenesis using the QuikChange mutagenesis kit (Stratagene) with the following primer and its reverse complement: ggaacatttagctctttctattctaatcatatagctaccatgg. Mutagenesis was confirmed by DNA sequence analysis. The protein was expressed, purified, and digested with TEV protease as previously described (3). It was then dialyzed against 25 mM Tris-HCl (pH 8.0) and 100 mM NaCl. Following dialysis, the sample was concentrated to 25 mg/ml as estimated by the absorbance at 280 nm (extinction

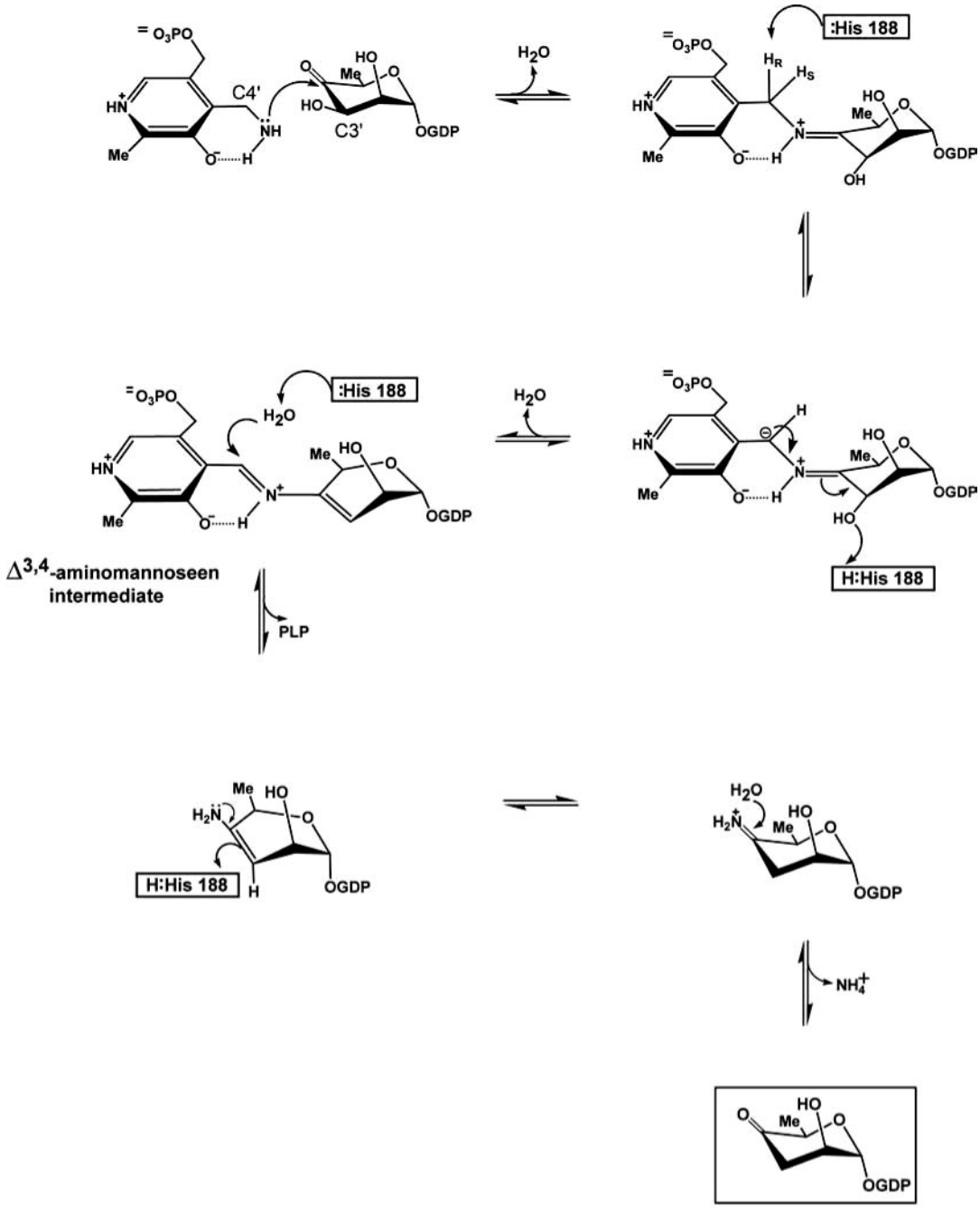

SCHEME 2. **A possible catalytic mechanism for ColD.**

coefficient of 0.98 $(mg/ml)^{-1}$ cm^{-1}, determined by the ProtParam tool from the Expasy Proteomics Server). The wild-type enzyme required for functional studies was expressed and purified as previously reported (3).

Production of GDP-Perosamine—Two enzymes were required for the production of GDP-perosamine, namely GDP-mannose 4,6-dehydratase and GDP-perosamine synthase. The GDP-mannose 4,6-dehydratase was prepared as previously described (5).

The gene *RfbE*, which encodes GDP-perosamine synthase, was isolated from the enterohemorrhagic strain of *Escherichia coli*, *O*157:*H*7 using a procedure identical to that previously described for the ColD gene (3). The resulting GDP-perosamine synthase-pET28JT plasmid was then used to transform HMS 174 *E. coli* cells (Novagen). Protein expression and purification were performed in a similar manner as that described for ColD (3).

GDP-perosamine was produced by reacting 5 mM GDP-mannose (Sigma), 20 mM glutamate, 1 mM PLP, 1 mM $NADP^+$, 3 μM GDP-mannose 4,6-dehydratase, and 1 μM GDP-perosamine synthase in Buffer A (50 mM HEPES, pH 7.5, and 50 mM NaCl). The reaction was incubated at room temperature for 2 h, after which it was heat-denatured for 2 min to precipitate the protein. The reaction mixture was then cooled on ice and centrifuged at 12,000 $\times$ *g* for 2 min, and the supernatant was removed from the protein pellet.

TABLE 1
X-ray data collection statistics

Parameters	Values
Space group	$P2_12_12_1$
Unit cell dimensions (Å)	$a = 62.4$, $b = 98.1$, $c = 119.9$
Resolution limits (Å)	30-1.7 (1.79-1.7)[a]
No. of independent reflections	75510 (9941)
Completeness (%)	92.4 (86)
Redundancy	5.8 (2.5)
Average I/average $\sigma(I)$	16.2 (3.2)
R_{sym} (%)[b]	8.5 (40.8)

[a] Statistics for the highest resolution bin are given in parentheses.
[b] $R_{sym} = (\Sigma|I - \bar{I}|/\Sigma I) \times 100$.

TABLE 2
Relevant least squares refinement statistics

Parameters	Values
Resolution limits (Å)	30-1.7
R-factor (overall) (%)/No. of reflections[a]	17.8/75,508
R-factor (working) (%)/No. of reflections	17.5/67,920
R-factor (free) (%)/No. of reflections	26.1/7588
No. of protein atoms	6231
No. of heteroatoms[b]	791
Average B values	
Protein atoms (Å^2)	20.4
PLP derivatives (Å^2)	24.5
Solvent (Å^2)	28.6
Weighted root mean square deviations from ideality	
Bond lengths (Å)	0.012
Bond angles (degrees)	1.7
Trigonal planes (Å)[c]	0.008
General planes (Å)	0.018
Torsional angles (degrees)	17.7

[a] R-factor = $(\Sigma||F_o| - |F_c||/\Sigma|F_o|) \times 100$, where F_o is the observed structure factor amplitude, and F_c is the calculated structure factor amplitude.
[b] These include 665 water molecules, two PLP derivatives, three ethylene glycol molecules, and eight sodium ions.
[c] The torsional angles were not restrained during the refinement.

The reaction supernatant was subsequently purified by an ÄKTA Purifier high performance liquid chromatography (HPLC) (Amersham Biosciences) equipped with a Resource-Q 6-ml anion exchange column (Amersham Biosciences). The column was first equilibrated with Buffer B (20 mM ammonium bicarbonate, pH 8.5), after which the reaction supernatant was loaded onto the column, washed, and eluted with a linear gradient to 60% Buffer C (500 mM ammonium bicarbonate, pH 8.5). The flow rate was 6 ml/min, and the elution was monitored at 253 nm. The fractions containing GDP-perosamine were pooled and freeze dried using a Labconco 1 L Freezone lyophilizer. Identity of the GDP-perosamine product was confirmed by ESI mass spectroscopic analysis (Mass Spectrometry/Proteomics Facility at the University of Wisconsin, Madison, WI). Solid GDP-perosamine was redissolved in water, and its concentration was determined by measuring the absorbance at 253 nm with an extinction coefficient of 1.38×10^4 M^{-1} cm^{-1}.

Crystallization of H188N ColD—Crystallization conditions were first surveyed by the hanging drop method of vapor diffusion using a sparse matrix screen developed in the laboratory. Large single crystals were subsequently grown via batch methods as previously described (3). The concentrations of the protein solutions were typically 25 mg/ml, and they contained 25 mM Tris (pH 8.0) and 100 mM NaCl. The precipitant solution contained 100 mM MES (pH 6.0), 28% polyethylene glycol 3400, 400 mM $MgCl_2$, 1 mM PLP, 2 mM α-ketoglutarate, and 10 mM GDP-perosamine. The crystals grew to maximum dimensions of $0.2 \times 0.5 \times 0.8$ mm in ~10 days and belonged to the space group $P2_12_12_1$ with unit cell dimensions of $a = 62.4$ Å, $b = 98.1$ Å, and $c = 119.9$ Å. The asymmetric unit contained the complete ColD H188N dimer.

X-ray Structural Analysis of H188N ColD—X-ray data were collected in house using a Bruker Proteum CCD detector system. The x-ray source was CuK_α radiation from a Rigaku RU200 x-ray generator operated at 50 kV and 90 mA. Single crystals were transferred in three steps to a cryoprotectant solution containing 30% polyethylene glycol 3400, 100 mM MES (pH 6.0), 500 mM $MgCl_2$, 100 mM NaCl, 15% ethylene glycol, 1 mM PLP, 2 mM α-ketoglutarate, and 30 mM GDP-perosamine. The crystals were then frozen in a cryostream, and an x-ray data set was collected from a single crystal. The x-ray data were processed with SAINT version 7.06A (Bruker AXS Inc., Madison, WI) and internally scaled with SADABS version 2005/1 (Bruker AXS). Relevant x-ray data collection statistics are presented in Table 1.

The structure of H188N ColD was solved via molecular replacement with the program EPMR (6) and employing the wild-type ColD structure as a search model (Protein Data Bank accession number 2GMU). All solvent molecules and the coordinates for His-188 and the PLP were omitted from the search probe. The resulting model was subjected to least-squares refinement with the program TNT (7). Model building was performed with the program Coot (8). Relevant refinement statistics are presented in Table 2. As observed in the wild-type ColD structure, residues Met-193, Val-334, and Asn-354 in both subunits adopted ϕ, ψ angles lying outside of the allowed regions of the Ramachandran plot, specifically in the "nucleophile elbow" region. Other than these, the Ramachandran statistics indicate that 90.7% of the residues adopt ϕ, ψ angles in the "most favored," 8.9% in the "additionally allowed," and 0.4% in the "generously allowed" regions.

ColD H188N Dehydratase Activity Assay—Typical ColD reactions contained 1 mM GDP-mannose, 2 mM L-glutamate, 0.2 mM PLP, 0.2 mM $NADP^+$, 3 μM GDP-mannose 4,6-dehydratase, and 1 μM ColD in Buffer A. Reactions were incubated at room temperature for 4 h and heat-denatured for 2 min to precipitate the protein. Samples were then cooled on ice and centrifuged at 12,000 $\times$ g for 2 min. Supernatants were removed and diluted 1:10 in water with 4% Buffer C.

ColD activity was qualitatively determined by analyzing reaction mixtures with mass spectrometry. The reactions were purified via HPLC. Diluted reactions were loaded onto the column and eluted with a linear gradient to 60% Buffer C. The flow rate was 2 ml/min, and the elution was monitored at 253 nm. Fractions from the peak corresponding to GDP-linked ketosugars (eluted at 185 mM ammonium bicarbonate) were pooled and lyophilized. Reaction contents were identified by ESI mass spectrometry.

GDP-Perosamine Assay—A reaction mixture containing 5 mM GDP-perosamine, 0.1 mM PLP, and 50 μM ColD wild-type protein was incubated at room temperature in Buffer A for 4 h. The reaction was heat-denatured for 2 min, cooled on ice, and centrifuged for 2 min at 12,000 $\times$ g. This reaction was repeated in the absence of ColD. The reaction contents were analyzed via HPLC. The column was equilibrated with Buffer B, and the

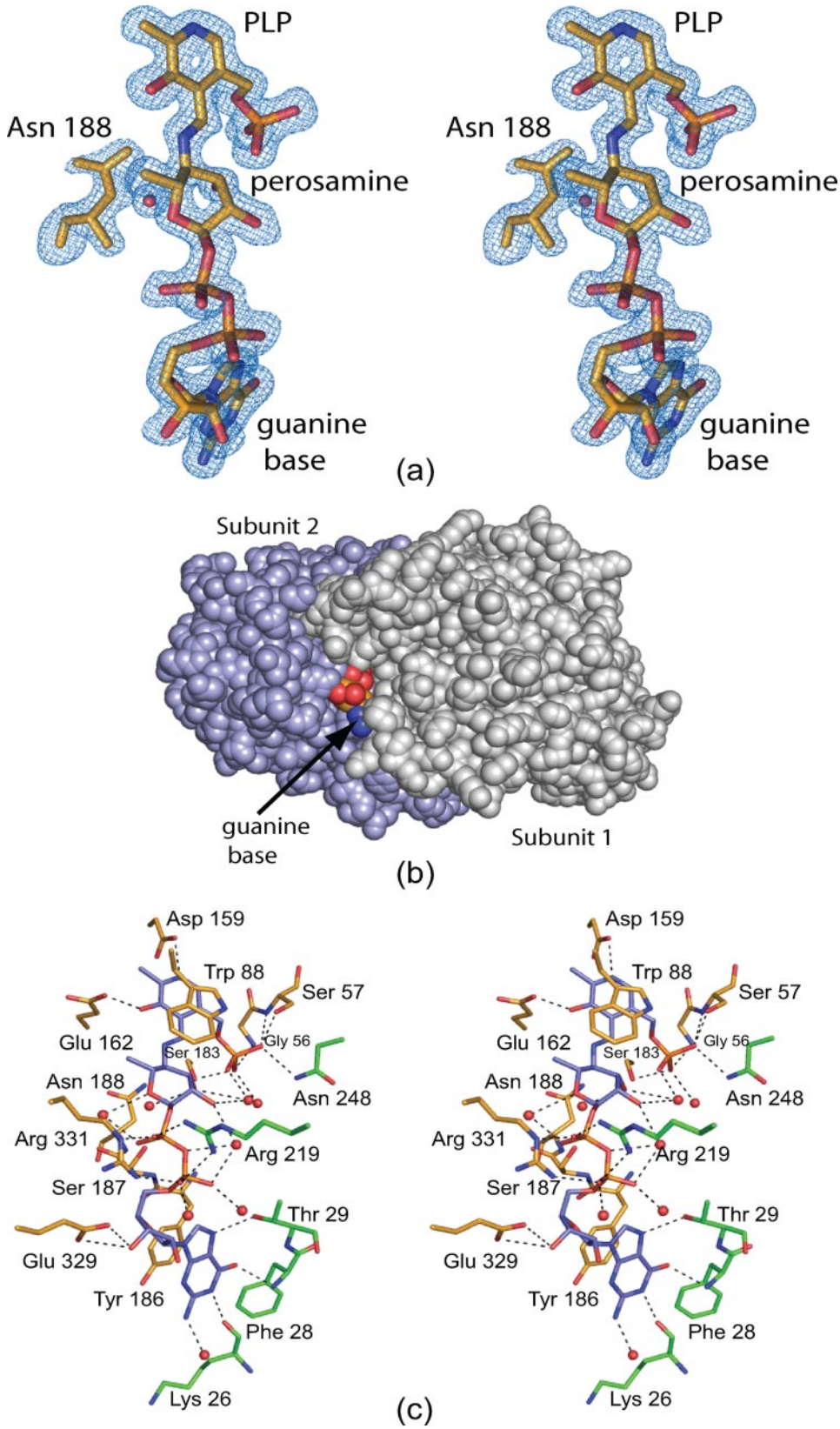

FIGURE 2. **Structure of H188N ColD.** Electron densities corresponding to the site of the mutation and the nucleotide-linked sugar are displayed in *stereo view* in *a*. The difference Fourier map was contoured at ~3σ and calculated with coefficients of the form ($F_o - F_c$), where F_o was the native structure factor amplitude and F_c was the calculated structure factor amplitude. A space-filling representation of the H188N ColD dimer is presented in *b*. Only the guanine base and several pyrophosphoryl oxygens of the nucleotide-linked sugar are solvent-exposed. A *stereo view* of the ColD active site is presented in *c*. Only those residues that lie within ~3.2 Å of the ligand are shown. The nucleotide-sugar ligand is highlighted in *blue bonds*, whereas those side chains contributed by Subunits 1 and 2 are displayed in *green* and *yellow bonds*, respectively. Possible hydrogen bonding interactions between the ligand and the protein or solvent are indicated by the *dashed lines*.

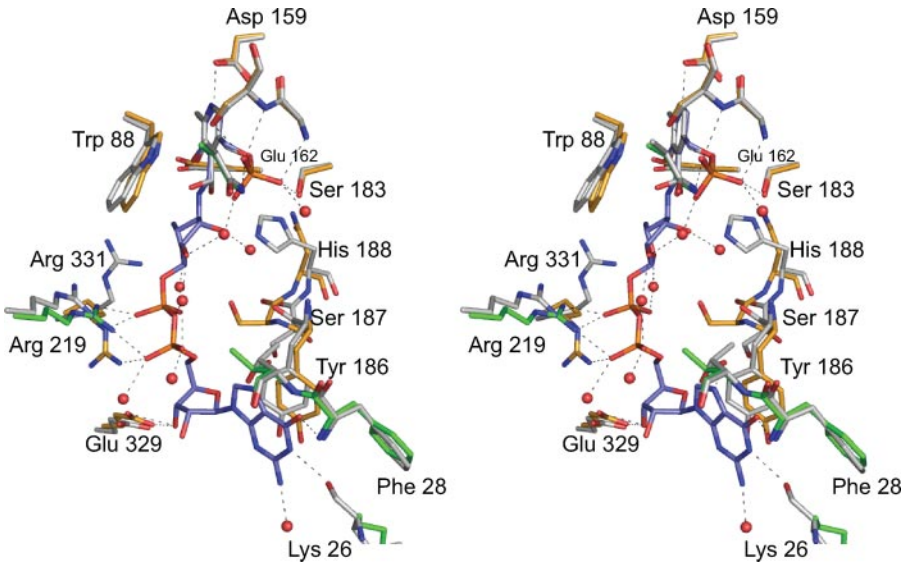

FIGURE 3. **Comparison of the wild-type and H188N ColD structures.** A superposition of the active sites for the wild-type and the H188N proteins is shown with the wild-type protein depicted in *white bonds* and the mutant protein shown as described in the legend to Fig. 2*c*.

reaction supernatant was loaded and eluted with a linear gradient to 100% Buffer C. The flow rate was 2 ml/min, and the elution was monitored at 253 nm. The contents of individual peaks were identified by ESI mass spectrometry.

RESULTS AND DISCUSSION

Overall, the electron densities corresponding to the polypeptide chain backbones for both subunits of the ColD dimer were well ordered. As expected, the conservative change of a histidine to an asparagine residue resulted in no gross structural perturbations. Indeed, the α-carbons for the wild-type and the H188N ColD proteins superimpose with a root mean square deviation of 0.6 Å using the algorithm described by Krissinel and Henrick (9). Given that the electron density was somewhat better for the second subunit in the x-ray coordinate file, however, the following discussion specifically refers to it unless otherwise indicated.

Shown in Fig. 2*a* is the electron density corresponding to the site of the mutation (H188N), the PLP cofactor, and the nucleotide-linked sugar. The nucleotide ribose adopts the $C_{2'}$-*endo* pucker, whereas the perosamine moiety assumes the $B_{2,5}$ rather than the more typically observed chair conformations. As depicted in Fig. 2*b*, the external aldimine is trapped within the active site cleft and is buried deeply between the two subunits of the dimer, with only a small portion of the guanine ring and the phosphoryl moieties exposed to the solvent.

A close-up view of the H188N ColD active site is presented in Fig. 2*c*. The guanine ring of the nucleotide is anchored to the protein via hydrogen bonds to the backbone carbonyl oxygen of Lys-26, the backbone amide group of Phe-28, and O^{γ} of Thr-29, all contributed by Subunit 1. A water molecule also lies within hydrogen bonding distance to the guanine ring. The 3′-hydroxyl group of the ribose hydrogen-bonds to the carboxylate of Glu-329, whereas the pyrophosphoryl oxygens interact extensively with four water molecules, the guanidinium group of Arg-219 from Subunit 1, and the guanidinium group of Arg-331 from Subunit 2. Strikingly, there are no specific interactions between the pyranosyl hydroxyls and the protein. Instead, water molecules serve to fulfill the hydrogen bonding potentials of these hydroxyls. The pyridoxal ring participates in hydrogen bonding interactions with both Asp-159 and Glu-162, and the phosphate moiety of the cofactor is positioned firmly in place by seven hydrogen bonds, three contributed by side chains (Ser-57 and Ser-183 from Subunit 2 and Asn-248 from Subunit 1), two from backbone amide groups (Gly-56 and Ser-57), and two from ordered waters. Trp-88 and Tyr-186 participate in stacking interactions with the pyridoxal ring of the cofactor and the guanine base of the nucleotide-linked sugar, respectively.

A superposition of the active sites for the wild-type and the H188N ColD proteins is presented in Fig. 3. Overall the active sites are similar with a few notable exceptions. First the side chain of Arg-331 in H188N ColD moves in toward the active site to interact with the pyrophosphoryl groups of the nucleotide-linked sugar. Second, the ψ angle of Tyr-186 flips from ~136° in the wild-type protein to −47° in the mutant enzyme, resulting in a change in orientation of the side chain for Ser-187. The other significant difference occurs at the site of the mutation. Whereas the imidazole group of His-188 is directed toward the active site in the wild-type enzyme, in the mutant protein, the asparagine side chain shifts slightly away. Importantly, in the mutant protein, a water molecule fills the space normally occupied by $N^{\epsilon 2}$ of His-188.

Wild-type ColD catalyzes the removal of the C3′-hydroxyl from the hexose ring via a ping-pong catalytic mechanism where in the first half PLP is converted to PMP via its reaction with L-glutamate. The second dehydration step results in the expulsion of the C3′-hydroxyl group (Scheme 2). To address whether the H188N ColD protein can catalyze this dehydration step, the following sets of experiments were conducted. First, the reaction of GDP-mannose with GDP-mannose 4,6-dehydratase (Scheme 1) without the addition of ColD was followed by ESI mass spectrometry, and the results are shown in Fig. 4*A*. The peak at 586.3 atomic mass units corresponds to GDP-4-keto-6-deoxymannose, the product of the dehydratase reaction. The additional peaks observed at 442.2 and 362.1 atomic mass units are fragmentation peaks corresponding to GDP and GMP, respectively. When the same reaction was carried out in the presence of wild-type ColD, the mass spectrum (Fig. 4*B*) indicated the conversion of the 586.3 atomic mass units peak into a new peak at 570.2 atomic mass units, which corresponds to GDP-4-keto-3,6-dideoxymannose. This conversion does not occur in the presence of H188N ColD (Fig. 4*C*), thus indicat-

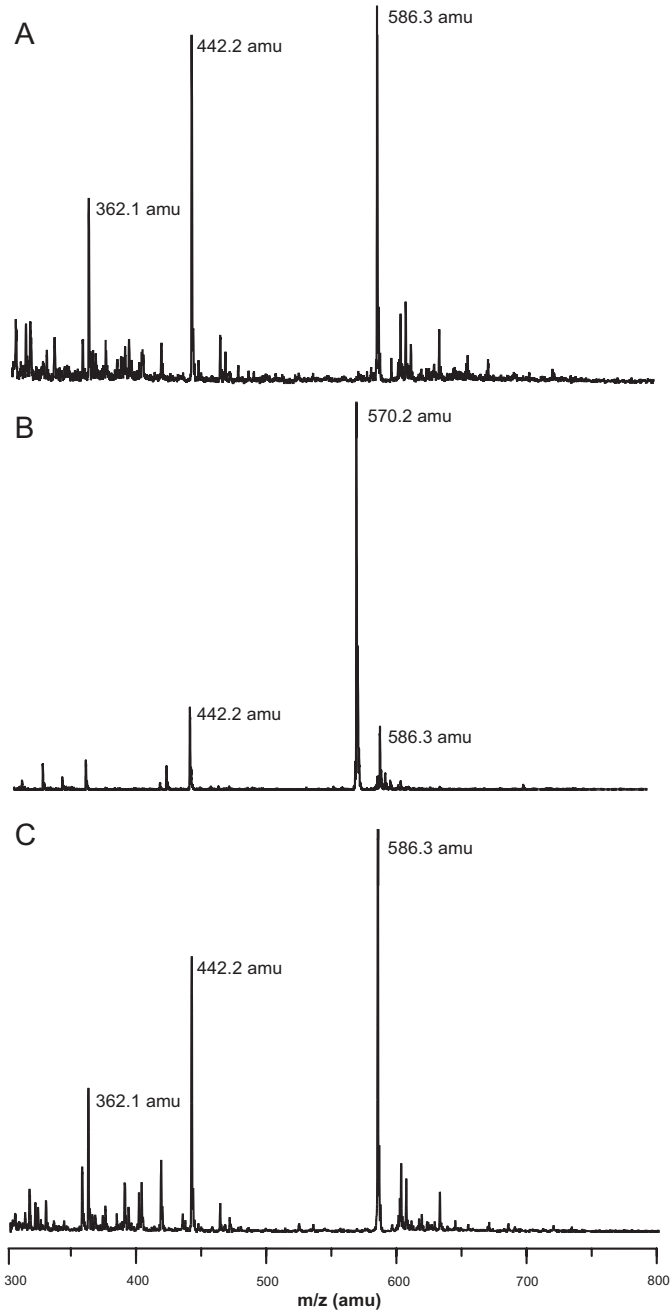

FIGURE 4. **ColD H188N dehydratase assay.** *A*, the reaction of GDP-mannose and GDP-mannose 4,6-dehydratase produces GDP-4-keto-6-deoxymannose (586.3 atomic mass units (*amu*)). This product partially fragments during mass spectroscopy, leading to the observed peaks at 442.2 and 362.1 atomic mass units, which correspond to GDP and GMP, respectively. The addition of wild-type ColD, shown in *B*, produces a new peak at 570.2 atomic mass units, which is the appropriate mass for the ColD product, GDP-4-keto-3,6-dideoxymannose. The same reaction carried out in the presence of the H188N mutant ColD demonstrates a buildup of the GDP-4-keto-6-deoxymannose substrate of ColD, with no conversion to product (*C*).

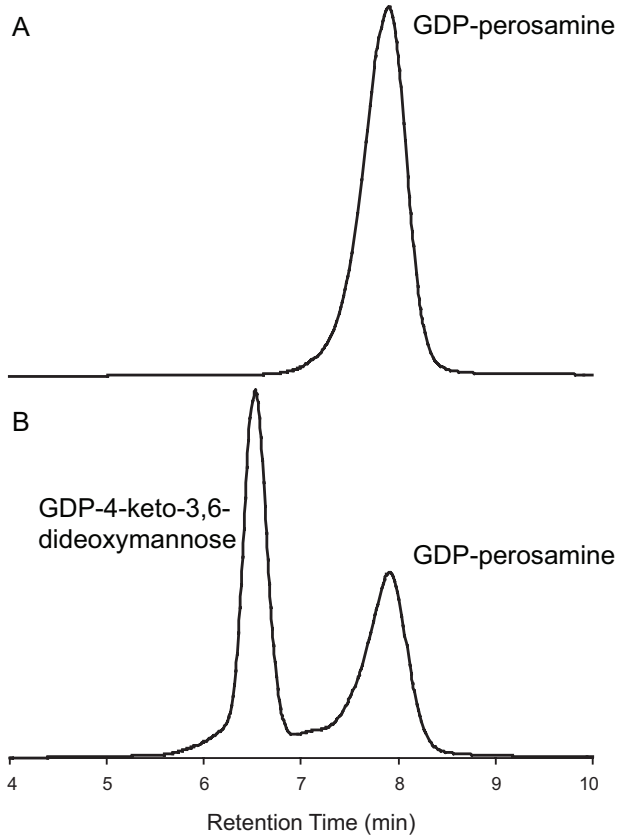

FIGURE 5. **GDP-perosamine assay.** The HPLC elution profile was monitored at 253 nm. The mixture of PLP and GDP-perosamine in *A* shows a single peak for GDP-perosamine at 7.9 min. The addition of wild-type ColD results in partial conversion of the GDP-perosamine peak to a new peak at 6.5 min, which was identified to be GDP-4-keto-3,6-dideoxymannose by mass spectrometry (*B*).

ing that the mutant protein cannot catalyze the second half of the ping-pong mechanism.

In our initial attempts to elucidate the structure of ColD with a bound sugar substrate, GDP-perosamine (Scheme 1) was added to wild-type ColD in concentrations of up to 20 mM. However, GDP-linked sugars were never observed at high enough occupancies to allow for their unambiguous placement into the electron density, although there were two rather large peaks that probably corresponded to the phosphoryl groups. It was reasoned that, perhaps, ColD was converting GDP-perosamine to GDP-4-keto-3,6-dideoxymannose, which was then simply dissociating from the enzyme.

To test this hypothesis, we incubated wild-type ColD with GDP-perosamine and PLP and in the absence of glutamate (the natural amino donor of ColD). Remarkably, ColD converted GDP-perosamine into the natural ColD product, GDP-4-keto-3,6-dideoxymannose (Fig. 5). Since GDP-perosamine is a 4-amino sugar, it can act as both the amino donor and the substrate of the dehydratase reaction. Given this additional activity of ColD, it explains why a mutant form of ColD was required to trap a GDP-linked sugar within the active site pocket. A possible mechanism for the conversion of GDP-perosamine to GDP-4-keto-3,6-didexoy-mannose is presented in Scheme 3. In this mechanism, the amino group at C4′ of the hexose forms a Schiff base with the PLP cofactor that is held in the ColD active site via noncovalent interactions. His-188 functions first as the base to abstract the hydrogen at the sugar C4′, leading to the formation of a quinonoid intermediate and its associated resonance forms and then as an acid to protonate the C3′-hydroxyl group. Upon protonation, the hydroxyl group departs resulting in the formation of the $\Delta^{3,4}$-aminomannoseen intermediate. At this stage, the catalytic mechanism is identical to that presented in Scheme 2.

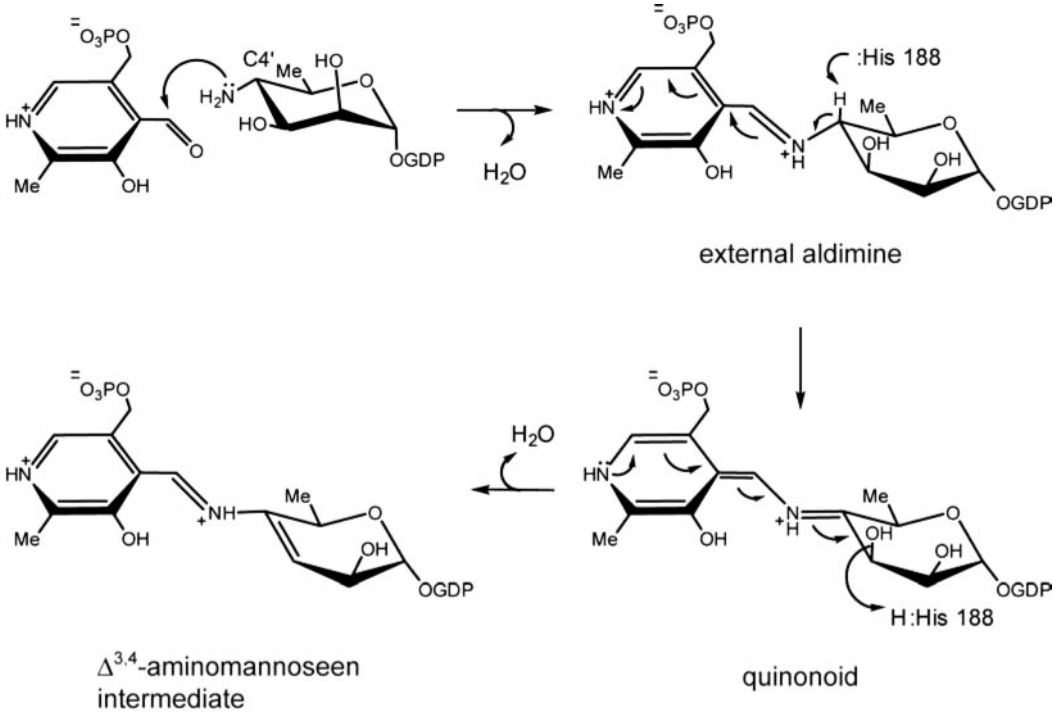

SCHEME 3. **A possible mechanism for the conversion of GDP-perosamine to GDP-4-keto-3,6-dideoxymannose.**

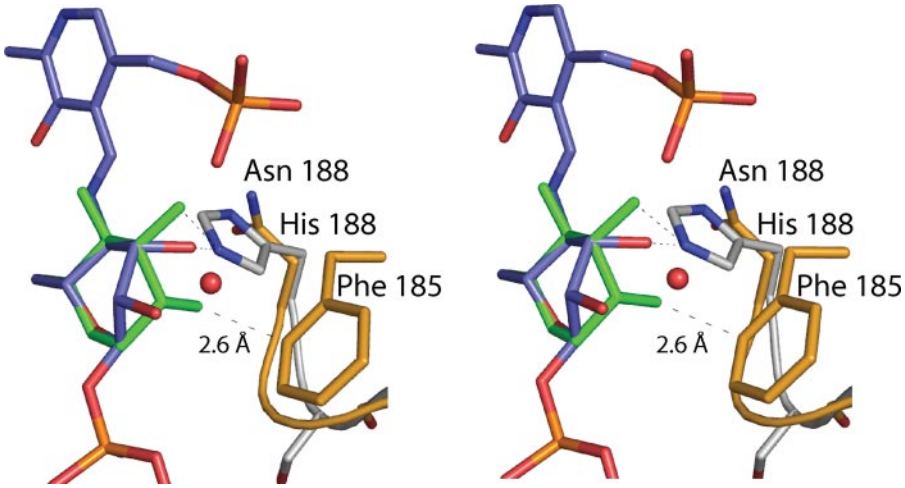

FIGURE 6. **Model of perosamine in the chair conformation.** The observed boat conformation of perosamine is depicted in *blue bonds*, whereas a model of the sugar in the chair conformation is displayed in *green bonds*. His-188 in the wild-type structure is depicted in *white bonds*, whereas Phe-185 and Asn-188 in the mutant protein are shown in *yellow bonds*.

Thus far, five additional x-ray crystallographic structures of sugar modifying aminotransferases have been reported: (*a*) ArnB from *Salmonella typhimurium*, a 4-amino-4-deoxy-L-arabinose lipopolysaccharide-modifying enzyme (10); (*b*) PseC, an aminotransferase from *Helicobacter pylori* that is involved in the biosynthesis of pseudaminic acid (11); (*c*) PglE, an enzyme responsible for amino transfer in the production of UDP-2,4-diacetamido-2,4,6,trideoxy-α-D-glucopyranose in *Campylobacter jejuni* (12); (*d*) DesI, the first aminotransferase involved in desosamine biosynthesis (13); and (*e*) DesV, the second aminotransferase in the desosamine biosynthetic pathway (14). Until the present report, only the structures of DesI and PseC were solved in the presence of nucleotide-linked sugars. Both of these enzymes transfer an amino group to the C4′ position of the sugar, albeit with differing stereochemistry, which most likely arises from the manner in which the sugars are oriented in the active sites (13). In both cases, the hexose moieties assume the $^4C_1$ conformations. Strikingly, in ColD, which functions as a dehydratase, the hexose adopts the less commonly observed $B_{2,5}$ conformation. Shown in Fig. 6 is a superposition of the observed boat conformation of perosamine and a model of the sugar in the $^4C_1$ conformation. Also included in Fig. 6 is the position of His-188 in the wild-type structure and the location of the water molecule that fills the cavity created when His-188 is replaced with an asparagine residue.

Why does perosamine adopt the boat conformation in the ColD active site? One reason might be due to steric hindrance from Phe-185 (Fig. 6). If the sugar adopted the $^4C_1$ conformation, its C2′-hydroxyl would be positioned within ~2.6 Å of the aromatic ring. The boat conformation might also arise from a variety of additional effects, including the manner in which the pyrophosphoryl oxygens of the nucleotide-linked sugar are coordinated by Arg-219 and Arg-331.

ColD is a PMP-dependent dehydratase, whereas ArnB, PseC, PglE, DesI, and DesV are PLP-dependent aminotransferases. Perhaps the adoption of the boat conformation somehow favors a dehydration reaction, or maybe the reaction specificity

results from a combination of subtle differences in the constellation of the active site residues. Experiments are presently under way to address this intriguing issue.

Acknowledgments—We thank Dr. Rodney Welch for graciously supplying the genomic DNA necessary for this research and Dr. James Thoden for continuing assistance throughout all stages of this investigation. We also thank Dr. W. W. Cleland for helpful comments.

REFERENCES

1. Lerouge, I., and Vanderleyden, J. (2002) *FEMS Microbiol. Rev.* **26,** 17–47
2. Raetz, C. R., and Whitfield, C. (2002) *Annu. Rev. Biochem.* **71,** 635–700
3. Cook, P. D., Thoden, J. B., and Holden, H. M. (2006) *Protein Sci.* **15,** 2093–2106
4. Alam, J., Beyer, N., and Liu, H. W. (2004) *Biochemistry* **43,** 16450–16460
5. Cook, P. D., and Holden, H. M. (2007) *Biochemistry* **46,** 14215–14224
6. Kissinger, C. R., Gehlhaar, D. K., and Fogel, D. B. (1999) *Acta Crystallogr. Sect. D* **55,** 484–491
7. Tronrud, D. E., Ten Eyck, L. F., and Matthews, B. W. (1987) *Acta Crystallogr. Sect. A* **43,** 489–501
8. Emsley, P., and Cowtan, K. (2004) *Acta Crystallogr. Sect. D Biol. Crystallogr.* **60,** 2126–2132
9. Krissinel, E., and Henrick, K. (2004) *Acta Crystallogr. D Biol. Crystallogr.* **60,** 2256–2268
10. Noland, B. W., Newman, J. M., Hendle, J., Badger, J., Christopher, J. A., Tresser, J., Buchanan, M. D., Wright, T. A., Rutter, M. E., Sanderson, W. E., Muller-Dieckmann, H. J., Gajiwala, K. S., and Buchanan, S. G. (2002) *Structure* (*Camb.*) **10,** 1569–1580
11. Schoenhofen, I. C., Lunin, V. V., Julien, J. P., Li, Y., Ajamian, E., Matte, A., Cygler, M., Brisson, J. R., Aubry, A., Logan, S. M., Bhatia, S., Wakarchuk, W. W., and Young, N. M. (2006) *J. Biol. Chem.* **281,** 8907–8916
12. Schoenhofen, I. C., McNally, D. J., Vinogradov, E., Whitfield, D., Young, N. M., Dick, S., Wakarchuk, W. W., Brisson, J. R., and Logan, S. M. (2006) *J. Biol. Chem.* **281,** 723–732
13. Burgie, E. S., and Holden, H. M. (2007) *Biochemistry* **46,** 8999–9006
14. Burgie, E. S., Thoden, J. B., and Holden, H. M. (2007) *Protein Sci.* **16,** 887–896